

Feasibility of using $\text{Ni}_{25}\text{Co}_{20}\text{Cu}_{10}\text{Fe}_{25}\text{Mn}_{20}$ high entropy alloy as a novel sintering aid in ZrB_2 ceramics



Samaneh Mamnooni^a, Ehsan Borhani^{a,*}, Mehdi Shahedi Asl^b

^a Department of New Science and Technology, Nanomaterials Group, Semnan University, Semnan, Iran

^b Department of Mechanical Engineering, Faculty of Engineering, Kyrenia, Mersin 10, Turkey

ARTICLE INFO

Keywords:

ZrB_2
Nano-crystalline
High entropy alloy
 $\text{Ni}_{25}\text{Co}_{20}\text{Cu}_{10}\text{Fe}_{25}\text{Mn}_{20}$
Spark plasma sintering
Sintering aid

ABSTRACT

For the first time, $\text{Ni}_{25}\text{Co}_{20}\text{Cu}_{10}\text{Fe}_{25}\text{Mn}_{20}$ high entropy alloy (HEA) was employed as a sintering aid for fabrication of ZrB_2 -based ceramics using spark plasma sintering (SPS) process. The mechanical properties, phase evolution, microstructural changes, and the densification mechanisms of ZrB_2 -5 wt% HEA ceramics during the SPS step were scrutinized. The ZrB_2 -5 wt% HEA ceramic, manufactured at 1900 °C, yielded interesting combination of properties, counting a relative density of 96%, a fracture toughness of 6.4 MPa m^{1/2}, and a hardness of 12.6 GPa. According to XRD patterns, there were ZrC and ZrO_2 phases with ZrB_2 matrix in the sintered samples. An unknown phase was also observed in the XRD patterns. Based on the history of the NiCoCuFeMn alloy and separation of Cu within the temperature range of 650–850 °C, that phase was related to CuB.

1. Introduction

There is limited number of natural elements with a melting point of above 3000 °C, such as carbon (C), rhenium (Re), tantalum (Ta) and tungsten (W). There are not many compounds containing this feature either. However, ultrahigh temperature ceramics (UHTCs) stand out dramatically [1–4] and numerous opportunities and advanced applications have been introduced. Accordingly, in recent years, detailed research has been conducted to develop UHTCs with good performance and boosted properties [5,6]. Among the ultra-high temperature ceramics, zirconium diboride (ZrB_2) has been widely studied due to its wide potential applications and attractive physicochemical properties. However, some issues related to ZrB_2 , such as low fracture toughness and poor sinterability, need to be solved [7,8]. In addition to an ultrahigh melting point (3245 °C), zirconium diboride has a relatively low density (6.1 g/cm³) and a set of excellent properties such as chemical inertness in touch with slags and molten metals, corrosion and erosion resistances in detrimental conditions, low thermal expansion coefficient, survival strength at elevated temperatures, high thermal shock resistance, as well as good thermal and electrical conductivities [9,10]. It has also been reported that ZrB_2 has good resistance to plasma arcs and sparks [11]. These features make ZrB_2 a viable option for usage in cutting-edge technologies such as microelectronics, cutting tools, solar absorbers, plasma-arc electrodes, and furnace elements. Due to the

inertness of ZrB_2 in contact with molten metals, this material is suitable for use in continuous casting of steels as refractory protective sleeve. ZrB_2 is also a good candidate for hypersonic vehicles, aerospace applications, jet vanes, nozzle components and wing leading edges [12–14].

The usage of monolithic ZrB_2 ceramic in industrial elevated temperature applications is limited due to weaknesses such as weak oxidation, damage, and ablation tolerance [15]. In addition, ZrB_2 has a low sinterability because of the presence of strong covalent bonds of Zr-B, low self-diffusion and oxide contamination such as zirconia (ZrO_2) and boria (B_2O_3) on the outer layer of ZrB_2 powders [16–19]. Dense ZrB_2 ceramics have been produced using hot pressing (HP) or hot isostatic pressing (HIP) under externally applied pressures at elevated temperatures. The production of ZrB_2 under these conditions requires costly electrical energy, post-processing procurement, sophisticated encapsulation technology, long preparation time, plus tooling and cutting to solve the shortage of the imperfect shaped samples and extra fabrication costs [20]. In addition, long holding time during sintering process reduces the structural properties due to grain growth and microstructure coarsening [20]. For the reasons mentioned above, use of sintering aids and a fast-sintering process such as spark plasma sintering is an effective way to overcome the weaknesses of ZrB_2 . The SPS method is a new method for densification of ceramic materials, which is also utilized for ultrahigh temperature ceramics. With this method, dense ceramics can be obtained with a short holding time, a fast-heating rate, and a

* Corresponding author.

E-mail address: e.borhani@semnan.ac.ir (E. Borhani).

Table 1

The list of publications utilizing HEAs as additive in ceramic-based materials.

Ceramic	HEA additive	Content	Advantages	Ref.
B ₄ C	CrMnFeCoNi	5 vol%	Lowered sintering temperature, improved strength, and hardness	[53]
TiB ₂	CoCrFeNiTiAl	5 wt%	Good wettability, no brittle phases, enhanced ductility, and densification	[55]
Ti(C,N)	AlCoCrFeNi	15 wt%	Enhanced toughness and hardness	[56]
TiC	Co _{1.5} CrFeNi _{1.5} Ti _{0.5}	20 wt%	Refined grains, improved toughness, and hardness	[57]
WC	Al _{0.5} CoCrCuFeNi	10-35 wt%	Improved hardness at room and high temperatures, enhanced toughness, inhibited grain growth	[50]
TiB ₂	CoCrFeNiAl	5 wt%	Promoted sinterability, excellent wettability, no brittle phases, enhanced mechanical properties, lowered sintering temperature	[58]
WC	AlFeCoNiCrTi	20 wt%	Inhibited grain growth, improved mechanical properties and corrosion resistance	[59]

relatively low processing temperature [21–26].

Numerous research works have been performed to provide dense ZrB₂ ceramics with great mechanical properties using press-assisted sintering techniques or sintering aids [27,28]. Non-metal additives such as SiC have been employed extensively to produce dense ZrB₂, but a high content of additive or intensely elevated sintering temperature is needed [29,30].

Meanwhile, metallic additives such as Nb [31], Fe [32,33], Mo [32,34], Ni [35,36], Cu [37], La [38], Cr [33], and Ti [39,40] have also been investigated. Although such additives can reduce the sintering temperature, they unfortunately result in decreased hardness. Some of the problems caused by the introduction of metal additives are summarized in the following. Adding Ni to ZrB₂ ceramics resulted in swelling, microcracks, and impossibility of approaching the full densification by

elevating the sintering temperature because of Ni evaporation [36]. Extensive swelling, microcracks and segregation were seen upon adding Cr to ZrB₂ ceramics [33]. Introducing Fe to ZrB₂ caused segregation, porosity, formation of Fe₂B brittle phase, Fe–Zr rich phase in grain boundaries and enhanced grain growth [33]. Incompatibility during the sintering process was reported when Nb was added to ZrB₂ [31]. Hence, it is necessary to discover novel additives that have the ability to diminish the sintering temperature while improving the properties.

One of the new types of novel additives that can lower the sintering temperature and prevent the grain growth of ceramics is HEA. It is actually defined as an alloy consisting of minimum five principal elements in an or near equimolar ratio, with a concentration range of 5 at% to 35 at% and a small atomic radius difference [41,42]. The ability to form a single solid solution phase or a combination of solid solution phases is characteristic of multicomponent systems or high entropy alloys where the formed phases have the same structures as the common structures of BCC, FCC and HCP [43]. Of course, in the case of improper

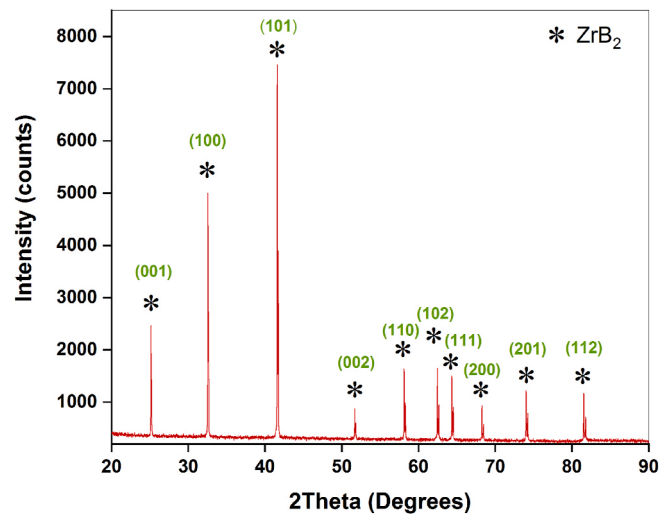


Fig. 2. XRD pattern of the raw ZrB₂ powder.

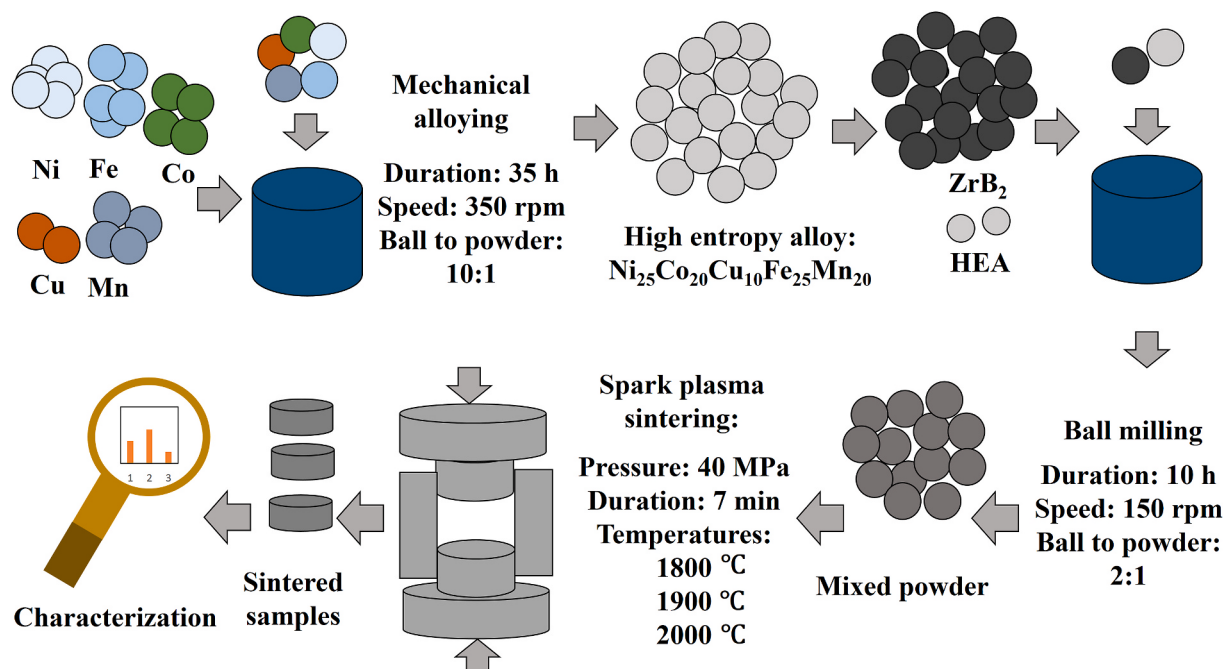


Fig. 1. Schematic illustration of the sample preparation steps.

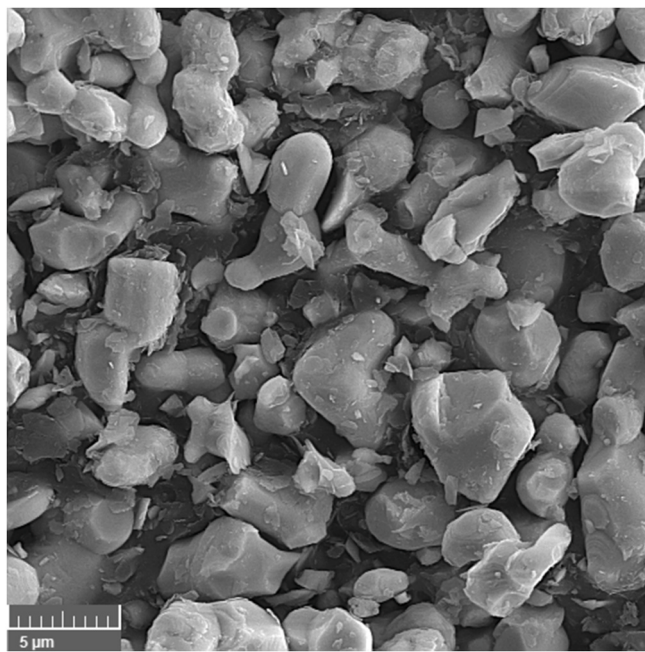


Fig. 3. FE-SEM image of the raw ZrB₂ powders.

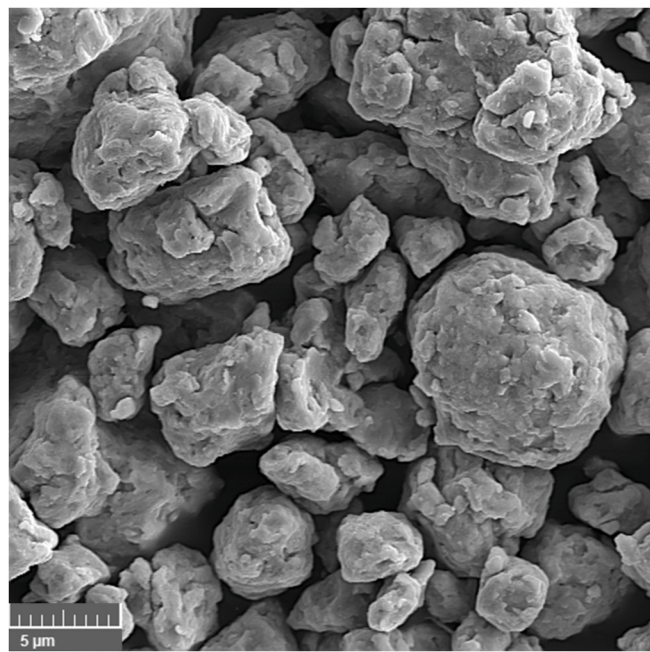


Fig. 5. FE-SEM image of the 35-h milled HEA powders.

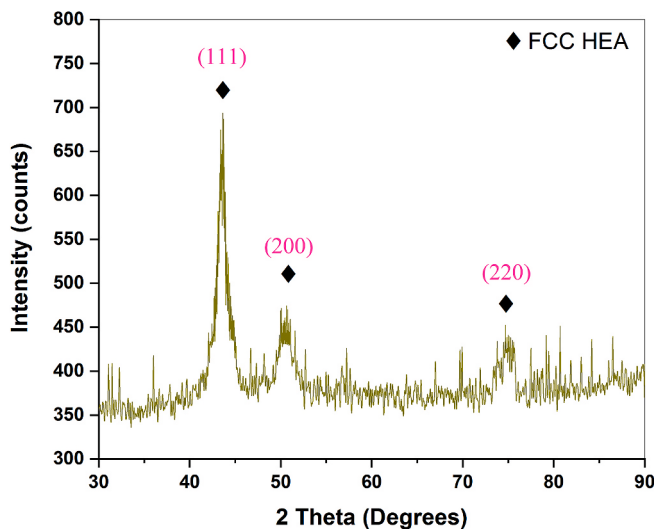


Fig. 4. XRD pattern of the HEA powder prepared via mechanical alloying (35 h milling).

design of alloy composition, it will not be possible to achieve a high entropy alloy with a single-phase solid solution structure [44]. The excellent characteristics of high entropy alloys such as wear resistance, good ductility, high toughness and strength, and thermal stability are directly attributed to the so-called “core effects”, which include high entropy, severe lattice distortion, cocktail effects, and sluggish diffusion [41,45–49]. HEA sinter additive is a suitable option for ceramics in order to reduce the sintering temperature, enhance the relative density and improve the mechanical behavior. For instance, upon applying Al_{0.5}CoCrCuFeNi and CoCrFeMnNi in WC [50,51], AlCoCrFeNi in Ti(C, N) [52], and CrMnFeCoNi in B₄C [53] strong materials with great mechanical properties were produced [54].

To the best of our knowledge, HEAs have not been used as sintering aids in ZrB₂-based ceramics. Additionally, the NiCoCuFeMn high entropy alloy has not been used as a binder in ceramics. As also mentioned earlier, the main problems of ZrB₂ ceramics are poor sinterability and

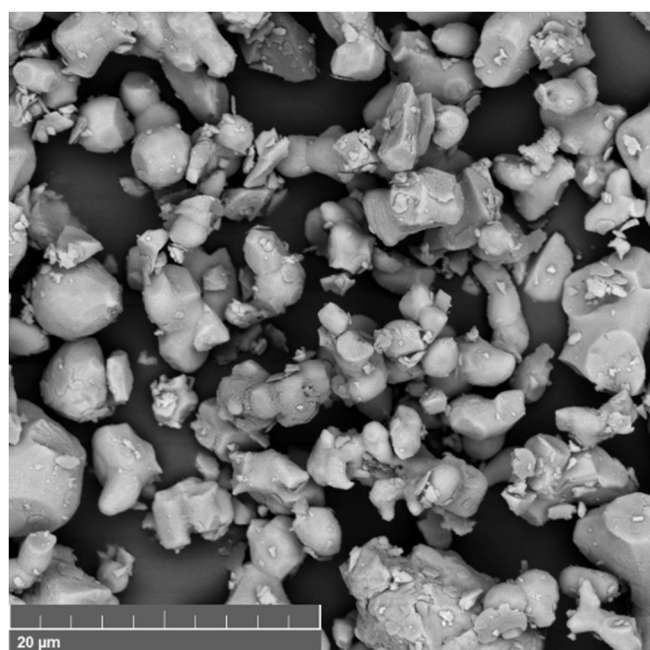


Fig. 6. FE-SEM image of the ZrB₂-5 wt% HEA mixture after ball milling process.

low fracture toughness [7,8]. Since the addition of an FCC high entropy alloy improved the fracture toughness of B₄C ceramics [53], it may be possible that the addition of an HEA improves the toughness of ZrB₂ ceramics. Table 1 lists the publications that have employed HEAs as the ceramic's binder. As seen, all HEAs contain the Cr element. It has been reported that the addition of Cr element to ZrB₂ ceramics has a negative effect on the microstructure [33]. Because of the possibility of Cr extraction from the HEA structure and its negative effect on ZrB₂ ceramics, we thus decided to use another element instead of Cr in HEA preparation. As the addition of Cu element has improved the mechanical properties of ZrB₂ ceramics [37], we made a decision to add the

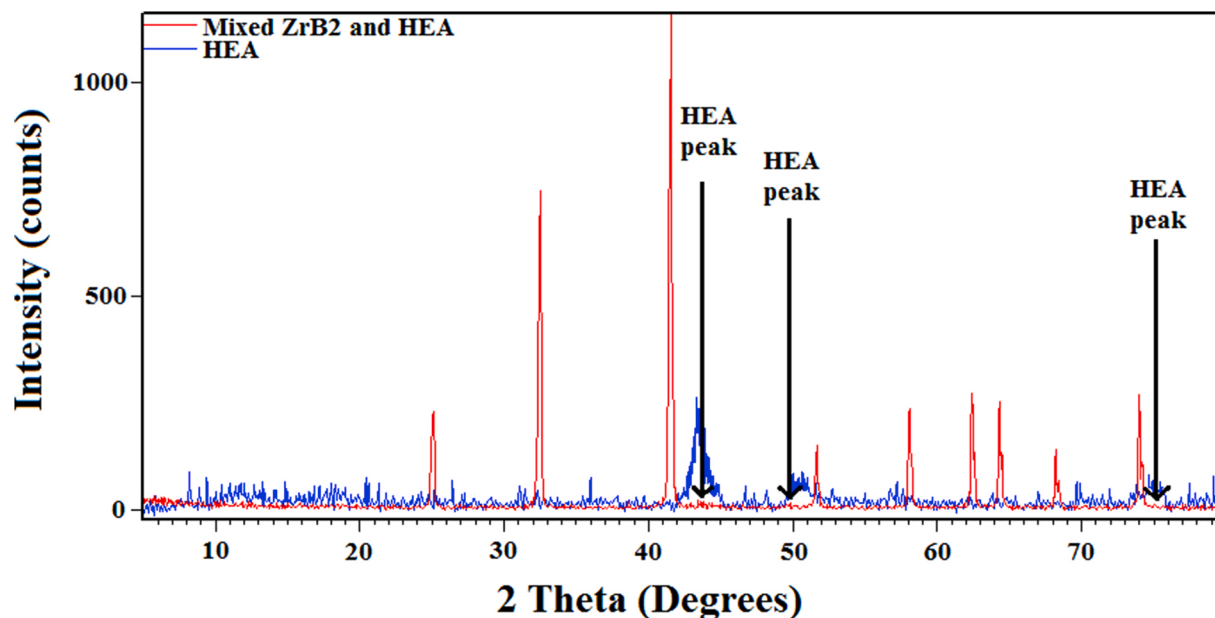


Fig. 7. XRD patterns of the as-mixed ZrB₂-5 wt% HEA together with the as-prepared HEA.

NiCoCuFeMn high entropy alloy as a sintering aid.

In the present study, a non-equiautomic Ni₂₅Co₂₀Cu₁₀Fe₂₅Mn₂₀ nanocrystalline HEA was first fabricated via mechanical alloying. Then, the ZrB₂-5 wt% HEA samples were prepared by ball milling and spark plasma sintering. The microstructure and mechanical characteristics of samples were characterized. The densification mechanisms of ZrB₂-5 wt% HEA ceramics were also studied.

2. Experimental steps

2.1. Sample preparation

Zirconium diboride (commercially available, purity: 99.5%, particle size:<10 µm, Pishro Ceramic Mehr) and HEA (synthesized by our group) powders were employed as starting materials. In order to mix the powders (95 wt% ZrB₂ and 5 wt% HEA), ball milling was carried out for 10 h at 150 rpm in a stainless-steel vial and balls with a ball-to-powder ration of 2:1. Note that according to Table 1, the HEA contents of 5–35% have been added to the ceramics in the published literature but in several cases, the amount of 5% seems to be appropriate to achieve excellent properties such high strength, hardness, ductility, and relative density. Thus, the additive content in our research was selected to be 5 wt%.

The ZrB₂-HEA materials were manufactured using a sintering furnace (SPS-20T-10). A die (graphite) with a diameter of 30 mm was used to compress the powders. The inner surfaces of the die and the surfaces of the punches were covered with flexible graphite foils. The sintering temperature range of 1800–2000 °C, dwell time of 7 min, applied pressure of 30 MPa, and heating rate of 120 °C/min were considered as SPS variables. A vacuum of 40 Pa was applied throughout the fabrication process. After finishing the SPS process, the device was turned off and the specimens were cooled down to the ambient temperature inside the furnace. Fig. 1 depicts a schematic illustration of the mentioned steps to provide a better perspective for the readers.

2.2. Characterization

After removing the outer layers of the samples through grinding, the bulk densities were calculated with the Archimedes method. The rule of mixtures was employed to calculate the theoretical densities. Then, relative density of the specimens was obtained through dividing bulk

density by theoretical density. The phase analysis of the ZrB₂-based ceramics was performed by X-ray diffraction (Philips PW3710 diffractometer) with Cu K_α ($\lambda = 0.154$ nm) radiation at step size/time of 0.02°/s. X'Pert HighScore Plus (version 3.0) and MAUD (Materials Analysis Using Diffraction 2017) were used for analyzing the XRD patterns and crystallite size. Before examining the microstructure and mechanical properties, the surface of the specimens was polished using sandpapers to obtain a mirror-like surface. The polished surfaces of the sintered ceramics were studied employing scanning electron microscopy (TESCAN MIRA 3) operated at 15.0 kV using backscattered electron (BSE) and secondary electron (SE) detectors. HSC Chemistry (9.3.0.9, Outotec) was applied for thermodynamics assessment. The hardness and fracture toughness were measured through the indentation technique utilizing the Vickers diamond pyramid (Wolpert, Germany) on the polished section by applying a load of 5 kg (49 N) for a dwelling time of 10 s. In order to calculate the indentation fracture toughness, the crack lengths, created by the Vickers indenter, were measured directly and embedded into the Anstis formula (Eq. 1) [60]:

$$K_{IC} = 0.016 \left(\frac{E}{H_V} \right)^{1/2} \left(\frac{L}{C^{3/2}} \right) \quad (1)$$

where E is the elastic modulus, L denotes the indentation force, H_V represents the Vickers hardness and C shows half of the crack length. The radial crack length was estimated using an optical microscope. The elastic modulus was estimated using an empirical equation, named Nielsen formula (Eq. 2) [61]:

$$E = E_0 \frac{(1 - P)^2}{1 + \frac{P}{\rho - 1}} \quad (2)$$

where E₀ is the theoretical modulus of a pore-free bulk, P reflects the amount of porosity, and ρ represents the Nielsen's shape factor (0.4).

3. Results and discussion

By observing the XRD pattern of the as-purchased ZrB₂ in Fig. 2, only ZrB₂ peaks can be found, thus confirming the purity of this material, which is also consistent with the supplier's claim. Although it is not visible in the XRD pattern, it has been proven that there are ZrO₂ and B₂O₃ layers on the surface of the ZrB₂ particles [62,63]. If those oxides

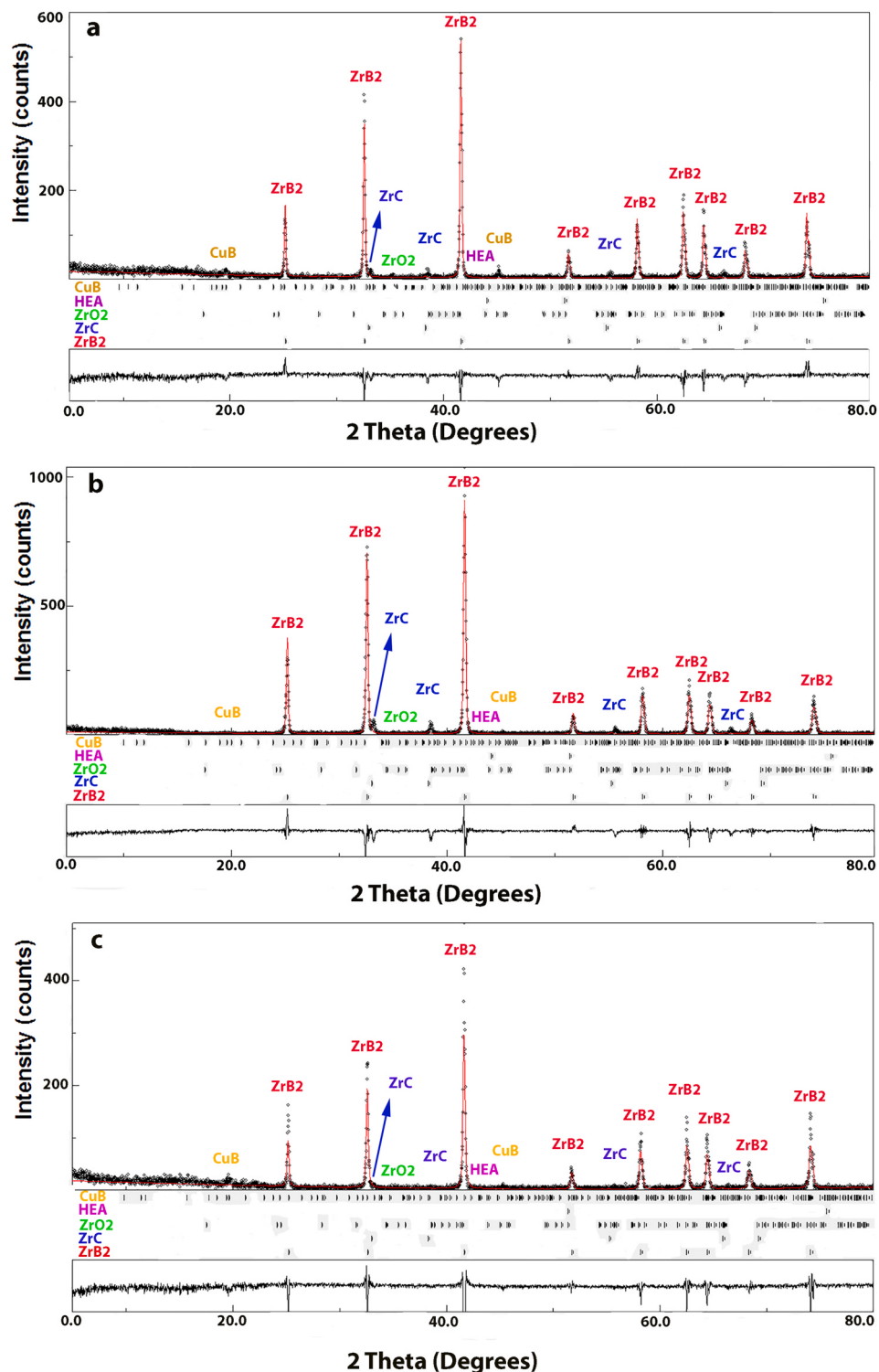


Fig. 8. XRD patterns of the ZrB₂-5 wt% HEA samples sintered at (a) 1800 °C, (b) 1900 °C, and (c) 2000 °C.

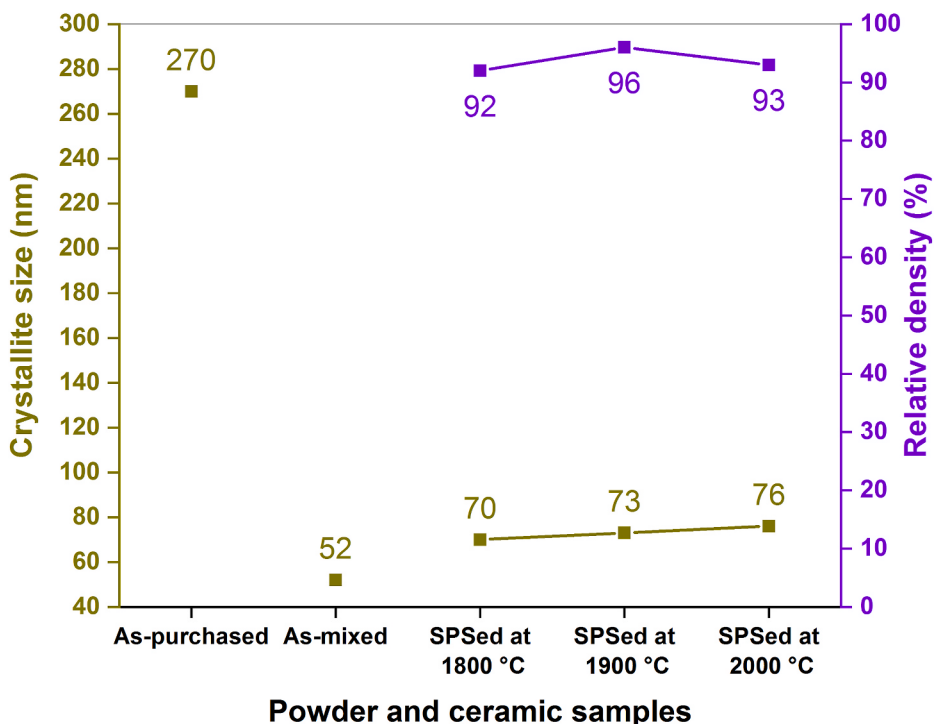


Fig. 9. Crystallite size of ZrB₂ in the as-purchased powder, as-mixed powder, and as-sintered samples as well as the relative density of sintered ceramics.

are not reduced during the sintering process, they will cause unfavorable effects such as weak interfaces and grain coarsening [64–66].

According to the FE-SEM image of the ZrB₂ powder (Fig. 3), the average particle size is approximately <10 µm, which is in accordance with the manufacturer's claim, and the morphology of the particles is also irregular.

The XRD pattern related to the high entropy alloy, after 35 h of milling process, is depicted in Fig. 4. As can be seen, this pattern has no peaks related to pure elements or intermetallic compounds, and the existing peaks are related to an FCC single solid solution. According to this pattern, it is clear that the mechanical alloying was successful in obtaining a nanostructured high entropy alloy in the Ni₂₅C₀₂₀Cu₁₀Fe₂₅Mn₂₀ system.

The FE-SEM image of the HEA powder is also demonstrated in Fig. 5, which shows a semi-spherical morphology with an average particle size of 8 µm. The size of the crystallites (9 nm) and the melting point (1100 °C) of the HEA were evaluated using the Debye Scherer method and DTA analysis (not reported here), respectively.

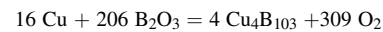
Fig. 6 indicates the FE-SEM image of the ZrB₂-5 wt% HEA mixture, which reveals the role of the ball milling on the homogeneous distribution of the particles and the relative reduction of the powder particle size due to the fracture caused by ball collision. Nevertheless, some agglomeration can also be seen in this image.

Fig. 7 presents the XRD pattern of the ZrB₂-5 wt% HEA powder after mixing via ball milling together with the pattern of the as-prepared HEA to help accurately identify trace phases in the mixture. According to the patterns, the peaks attributed to HEA are very weak and difficult to recognize but the sharp peaks are all related to the ZrB₂ phase. This can be due to the fact that the HEA is a random solid solution and because of the production method (mechanical alloying is a severe plastic deformation route), it has a strong lattice distortion. In addition, the amount of added HEA to ceramic is also very low (5 wt%). Owing to the mentioned reasons, the diffraction peaks of the HEA are too weak. Since no extra peak was identified in the pattern related to mixed powder, no reaction between the alloy and ceramic occurred during the mixing process. Also, by comparing the XRD patterns of the raw ZrB₂ and ZrB₂-5 wt% HEA mixture, it can be seen that after mixing, the width and

intensity of the ZrB₂ phase peaks have increased and decreased, respectively. These observations have occurred in response to the milling process and due to one of the following reasons: high lattice strain, grain refinement, or reduced crystallinity [67,68].

The XRD patterns of ZrB₂-5 wt% HEA ceramic samples sintered at different temperatures (1800–2000 °C) are given in Fig. 8. In all patterns, using the X'Pert HighScore Plus software, weak peaks of the HEA and several peaks of ZrC, ZrO₂ and CuB (Cu₄B₁₀₃) phases were identified along with the main phase of the ZrB₂. The formation of CuB phase may be attributed to the high temperature reaction of ZrB₂ surface oxide (B₂O₃) with elements dissolved in the HEA. The presence of ZrO₂ and ZrC phases can also be attributed to the formation of the oxide shell on the surface of the initial ZrB₂ particles, where part of the oxide layers has been reduced to carbide by the carbon absorbed from the sintering system (e.g. the graphite foil). Note that the presence of brittle secondary borides (M₂B, M₂₃B₆) in the XRD patterns was not confirmed, so the final product may have good mechanical properties.

According to the literature, in the NiCoCuFeMn HEA system, copper element has a large atomic radius and the enthalpy of mixing of this element with the next four elements is positive. Therefore, copper does not mix with other elements in the alloy. At the temperature range of 650–850 °C, γ phase (Cu-rich nanoclusters) segregates from system [70–72]. Within those temperatures, the B₂O₃ phase (impurity on the surface of ZrB₂ particles) is liquid. CuB phase is probably formed due to the following reaction (Eq. 3) in the system. The probability of this reaction occurring at the temperature range of the sintering process was investigated using HSC Chemistry software. Unfortunately, no data related to the CuB phase were found in the database of this software. The sluggish diffusion effect, which is one of the four core effects associated with high entropy alloys and slowing down reactions, is rejected for NiCoCuFeMn HEA [72]. Thus, the formation of such boride phase (CuB) due to the high temperature reaction of the ceramic matrix with the elements separated from the high entropy alloy can be predicted. Possibly, the formation of CuB boride phase improves the sinterability of ZrB₂ [53].



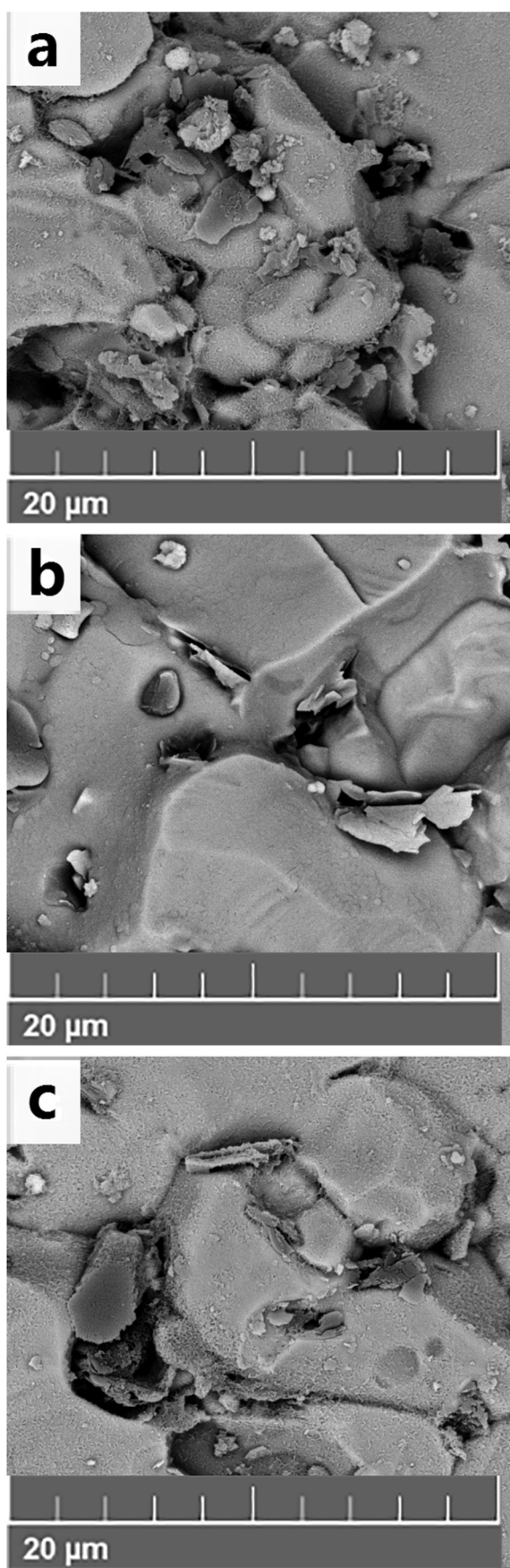


Fig. 10. Grain size evolution at different SPS temperatures: (a) 1800, (b) 1900, and (c) 2000 °C.

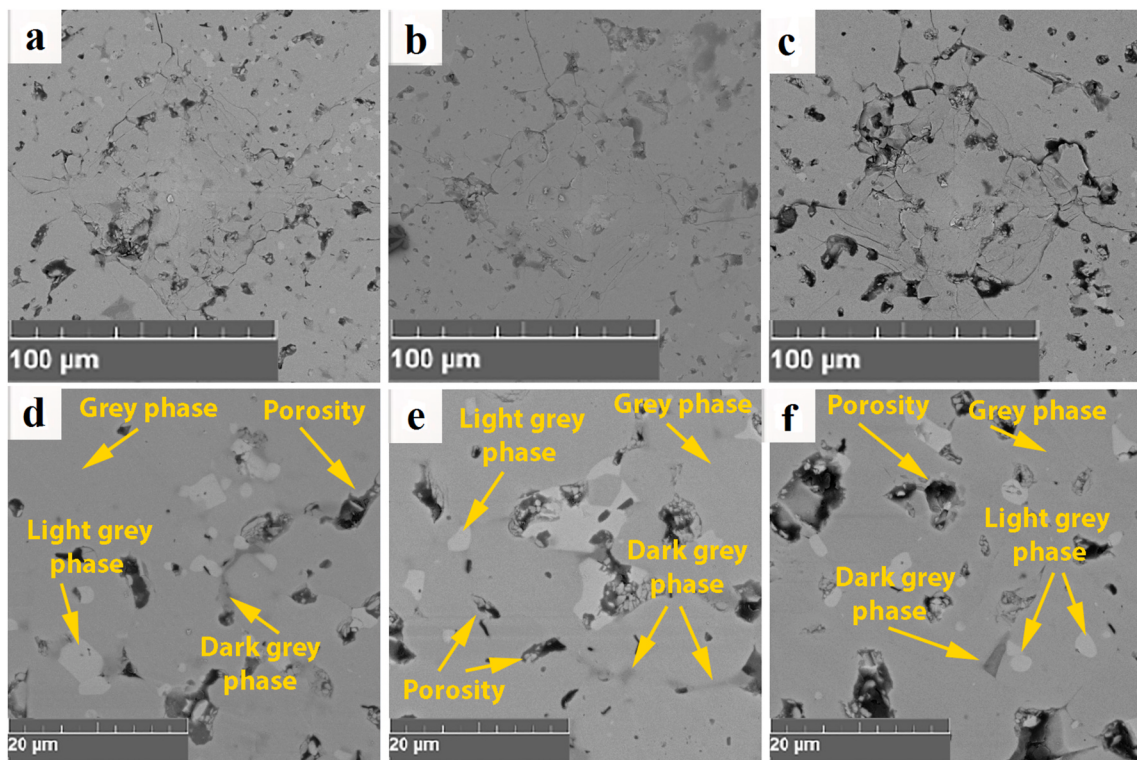


Fig. 11. Backscattered electron FE-SEM images of polished surface of ZrB_2 -5 wt% HEA samples sintered at various temperatures: (a,d) 1800 °C, (b,e) 1900 °C, and (c,f) 2000 °C.

By comparing the XRD patterns of ZrB_2 -5 wt% HEA, before and after sintering at various temperatures, it is noticeable that the width of the peaks has diminished with elevation of the temperature. The reason for this observation may be related to the release of lattice strain and coarsening of crystallite size. In order to accurately investigate these changes, the crystallite size of ZrB_2 phase was calculated using the width of the XRD peaks and the Debye-Scherer formula (changes are illustrated in Fig. 9). According to the curve, it can be seen how much the ball milling method is useful in reducing the size of the crystallites. Also, the mechanical combination of powders, besides reducing the size of the particles, augments the reactivity of the powders [73]. The increase in surface area due to the reduction in particle size acts as a driving force for promoting densification [74]. After sintering at different temperatures, the crystallite size of the ZrB_2 phase is slightly increased, but even with sintering at a high temperature of 2000 °C, the size of the crystallites is still below 100 nm. Fig. 10 presents the SEM images revealing the grain size evolution at different sintering temperatures. It seems that the grain size does not differ much at different SPS temperatures, which is consistent with the crystallite size variations (Fig. 9).

The relative density values of the fabricated samples at temperatures of 1800, 1900, and 2000 °C were calculated as 92%, 96%, and 93%, respectively (Fig. 9). The presence of HEA contributed to achieving relative densities higher than 92% at different sintering temperatures. Meanwhile, for the monolithic ZrB_2 sample, the densities obtained at this temperature range were significantly lower [15]. Since the melting temperature of the HEA (1100 °C mentioned before) is far lower than the range of the SPS process (1800–2000 °C), the HEA plays an important role in promoting densification through the mechanism of liquid phase formation. Thus, according to these results, the presence of HEA boosted the sintering process. Also, upon moving between the particles, the HEA improved the overlapping between the particles, enhanced the grain boundary diffusion, and also filled the pores. It has been reported that the HEA can create new phases and improve sinterability through a series of chemical reactions [75]. With temperature elevation from 1800 °C to 1900 °C, the densification was improved (from 92% to 96%),

but with a further increase in the temperature to 2000 °C, the relative density dropped to 93%. This decline in relative density by performing the SPS process at 2000 °C is probably related to the increase in porosity content due to the growth of ZrB_2 grains [76]. Meanwhile, there is a possibility of increasing porosity content due to the evaporation of the elements separated from the high entropy alloy at a relatively high temperature of 2000 °C.

Fig. 11 illustrates the backscattered electron FE-SEM images of the polished sections of ZrB_2 -5 wt% HEA specimens after sintering process at various temperatures (1800–2000 °C). Upon increasing the temperature to 1900 °C, the percentage of porosities was reduced, indicating the progression of the sintering process. As an outcome of creating bonds between the particles, open pores are reduced and become isolated pores. Indeed, with elevation of the sintering temperature, the porosities are removed from the grain boundaries and triple junctions. However, with further increase in the temperature to 2000 °C, the porosity content was enhanced.

According to Fig. 11, three distinct phases (grey, light grey and dark grey) are seen in all samples. In order to identify such phases in the samples, EDS maps taken from the polished and fracture surfaces of the sample SPSed at 1900 °C are shown in Fig. 12 a and 12 b, respectively. According to the EDS analysis of the polished surface, it is clear that the grey phase corresponds to the ZrB_2 , the dark grey is related to HEA, and the light grey is related to ZrC .

Based on the EDS results of the fracture surface (Fig. 12 b), it can be recognized that four elements of Fe, Mn, Ni and Co have a uniform distribution, but Cu has a different distribution (sites indicated by arrows in Fig. 12 b). The lower presence of Cu element, in places where other elements (Fe, Mn, Ni and Co) are present, can be attributed to the lower atomic percentage of this element in the composition of the $\text{Ni}_{25}\text{Co}_{20}\text{Cu}_{10}\text{Fe}_{25}\text{Mn}_{20}$ HEA. In addition, the presence of copper in places where the boron is also available can be a sign of the separation of copper from the HEA and the formation of CuB phase.

Fig. 13 depicts the fracture surfaces of the sintered samples at 1800–2000 °C. According to the fracture surface of the sintered sample at

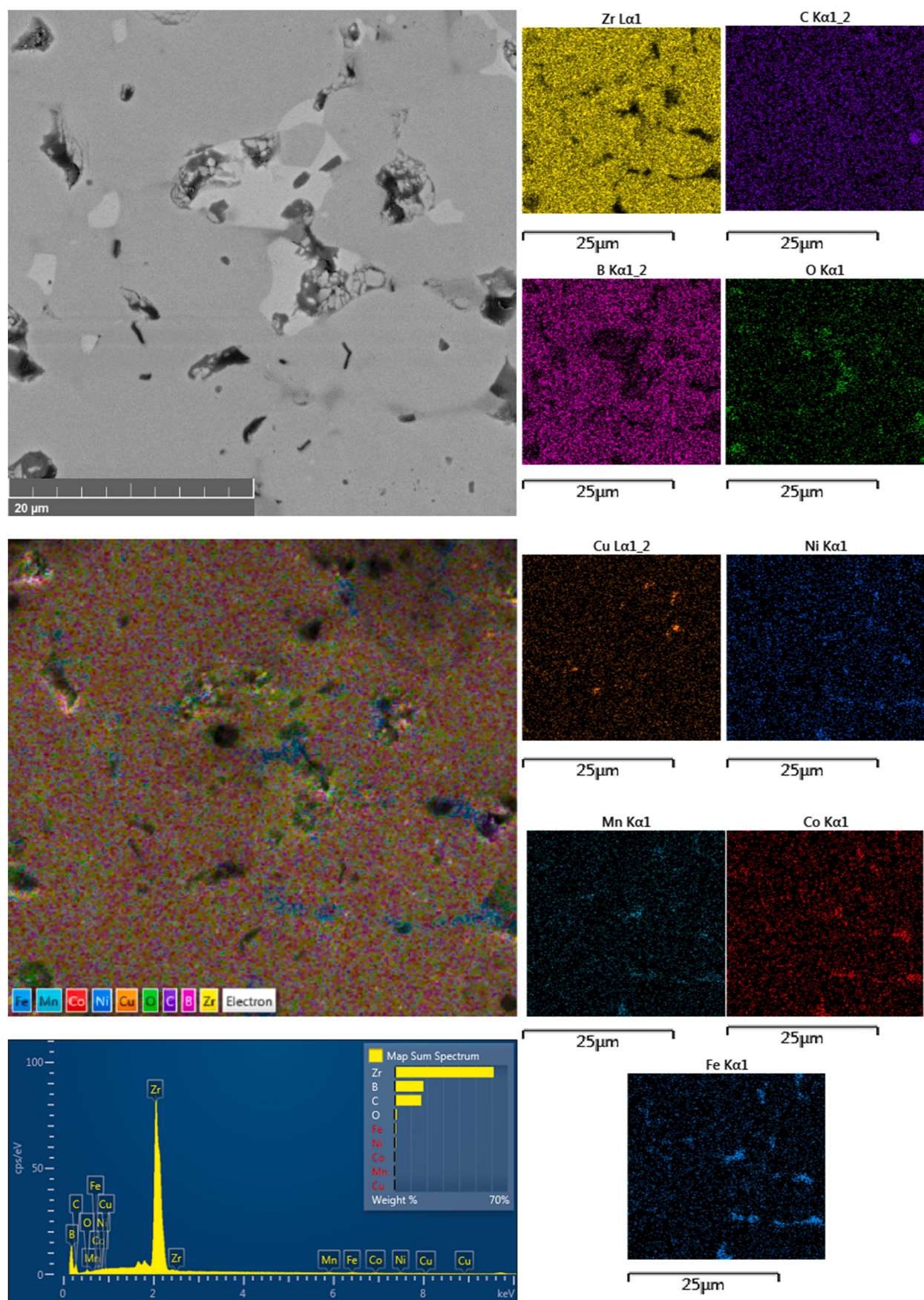


Fig. 12 a. EDS map analysis from the polished surface of the sample sintered at 1900 °C.

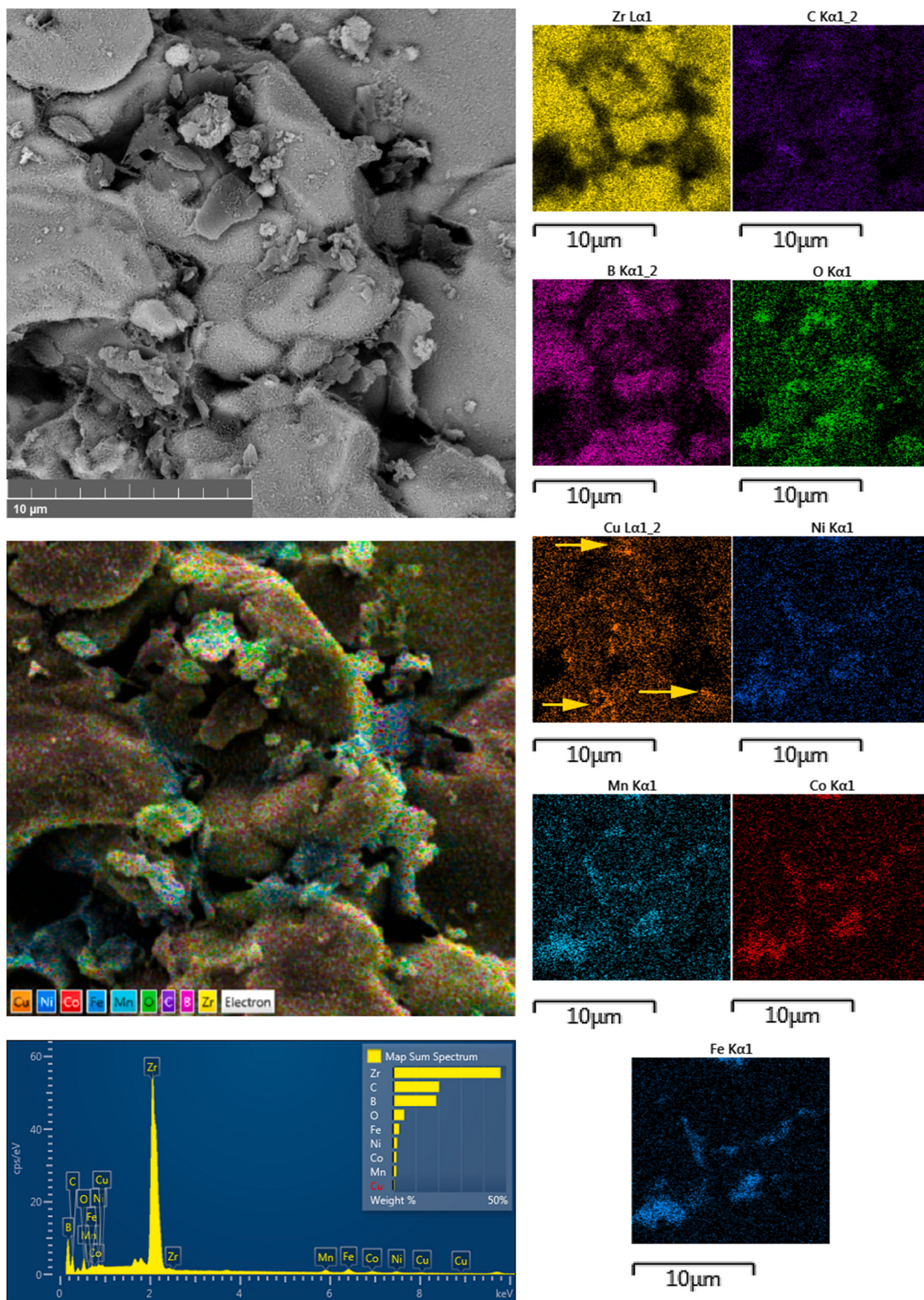


Fig. 12 b. EDS map analysis from the fracture surface of the sintered sample at 1900 °C.

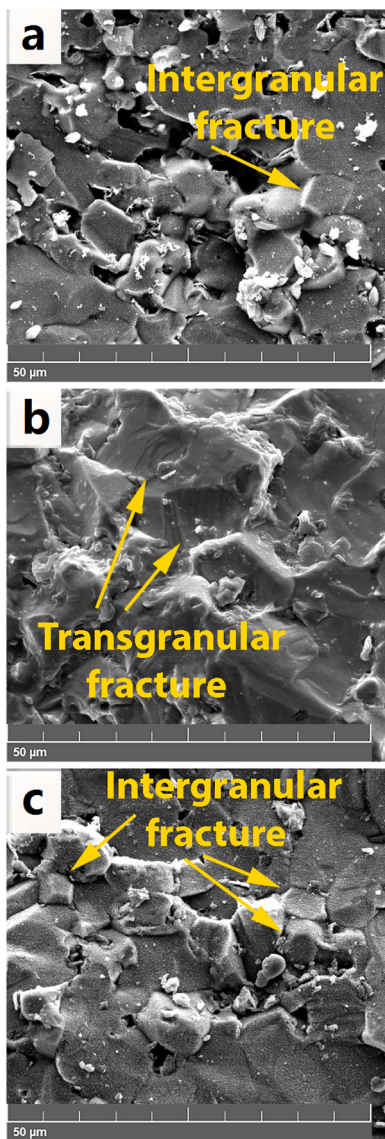


Fig. 13. Secondary electron FE-SEM images of the fracture section of ZrB₂-5 wt % HEA samples sintered at (a) 1800 °C, (b) 1900 °C, and (c) 2000 °C.

1800 °C (Fig. 13a), a large number of pores and interconnected necks can be seen, suggesting that the sintering process is in the early stages. The dominant mode of fracture in this sample is intergranular, which occurs due to the large extent of porosity in the sample and the insufficient temperature of the sintering. In the intergranular mode, the fracture occurs at the grain boundaries, but in the transgranular mode, the grain itself breaks. The intergranular fracture indicates insignificant progress in the sintering process as no noticeable grain boundary has formed yet among the particles. The densification mechanisms at this temperature (1800 °C) include the mechanical cohesion and rearrangement of particles.

According to the fracture surface of the sintered sample at 1900 °C (Fig. 13b), it can be seen that the bond between the particles has increased, and a small amount of porosity can be seen in the fracture surface, indicating the progression of the sintering process. Upon heightening the sintering temperature to 1900 °C, the fracture type has changed to a combination of intergranular and transgranular modes. Meanwhile, the transgranular fracture mode is dominant, which indicates a strong bond between the ZrB₂ grains together and with the HEA. The presence of river patterns indicates transgranular fracture mechanism [77]. There was a proper wettability between ZrB₂ and HEA,

so the additive worked well as a sintering aid, and good mechanical properties can be predicted for this sample [53].

Based on the fracture surface of the sintered sample at 2000 °C (Fig. 13c), it is noticeable that the progression of the sintering process is better than that of the sample sintered at 1800 °C but worse than the one sintered at 1900 °C. The fracture type is a combination of intergranular and transgranular modes, in which the intergranular mode is dominant. Upon increasing the sintering temperature, grain growth can be expected, but it is not noticeable even at 2000 °C. This may be due to the presence of high entropy alloy, which stops the migration of ZrB₂ grain boundaries via pinning mechanism and prevents significant grain growth. In addition, there is also the possibility of slowing down the grain growth through the removal of surface oxide impurities such as B₂O₃ due to the reaction with the Cu element (Eq. 3) [78].

Fig. 14 displays the displacement-time-temperature (DTT) curve related to the sample sintered at 1900 °C, taken during the SPS. Upon initiating the manufacturing process, a slight displacement is observed in 3–4 min, which is most likely related to the removal of gas from the inserted powders into the mold, after which a constant displacement is observed until 8 min. Next, with increasing the temperature and time, the displacement increased with a slight slope up to 1.1 mm, which seems to have happened with the beginning of the sintering process and the formation of a neck between the particles. Then the displacement grew with a steep slope up to 3.3 mm, and indeed, the main shrinkage occurred in the temperature range of 1800–1850 °C in less than 3 min. After this step, displacement increased with a moderate slope to the final value of 5.4 mm. The displacement curve was still ascending after reaching the maximum temperature (1900 °C) and did not reach a constant state again as with the beginning of the SPS. According to the relative density value (96%), this result is confirmed.

Fig. 14b and c demonstrate the displacement rate curves versus time and temperature for the sample sintered at 1900 °C, respectively. The displacement rate has two main peaks versus time and temperature. The first one is a weak peak at 4 min and 1000 °C, which is most likely related to the rearrangement of the particles or melting of the HEA. The second one is a sharp peak with a considerable displacement at the temperature range of 1800–1850 °C where the time range is 12–15 min. The results extracted from these two curves are also in agreement with the data obtained from the DTT curve. The starting shrinkage temperature (SST) extracted from the DTT curve for the sample sintered at 1900 °C was 1000 °C, which is significantly lower than that of the pure ZrB₂ sample (1570 °C) sintered at 1900 °C with almost similar sintering conditions [79]. This can be attributed to the lower melting temperature of the HEA (1100 °C) compared to the ZrB₂ (3245 °C), which has caused reduction of SST parameter [21].

The curve of hardness variations as a function of sintering temperature is presented in Fig. 15. Elevation of sintering temperature from 1800 °C (10.9 GPa) to 1900 °C (12.6 GPa) led to 30% hardening, but with a further rise in the temperature to 2000 °C, the hardness of the sample (10.3 GPa) dropped significantly. Generally, the hardness of a sample is affected by several parameters such as porosity, grain size, and secondary phases [80]. It is well established that the porosity in ceramics has no resistance against the applied stress, and therefore, the sample with greater porosity will have lower hardness than its denser counterpart [81]. It has also been proven that a ceramic sample with a larger grain size will have lower hardness than a fine-grained sample [81].

Fig. 15 indicates the fracture toughness variations as a function of SPS temperature. Augmentation of temperature from 1800 to 1900 °C caused a slight improvement in the fracture toughness, but further elevation of temperature to 2000 °C led to a negative outcome. Among the different parameters, crystallite size and porosity have the greatest effects on the fracture toughness of the ceramic samples [82]. Indeed, the higher hardness and fracture toughness of the sample sintered at 1900 °C compared to those sintered at 1800 °C and 2000 °C, can be attributed to its fine-grained and dense microstructure. The fracture

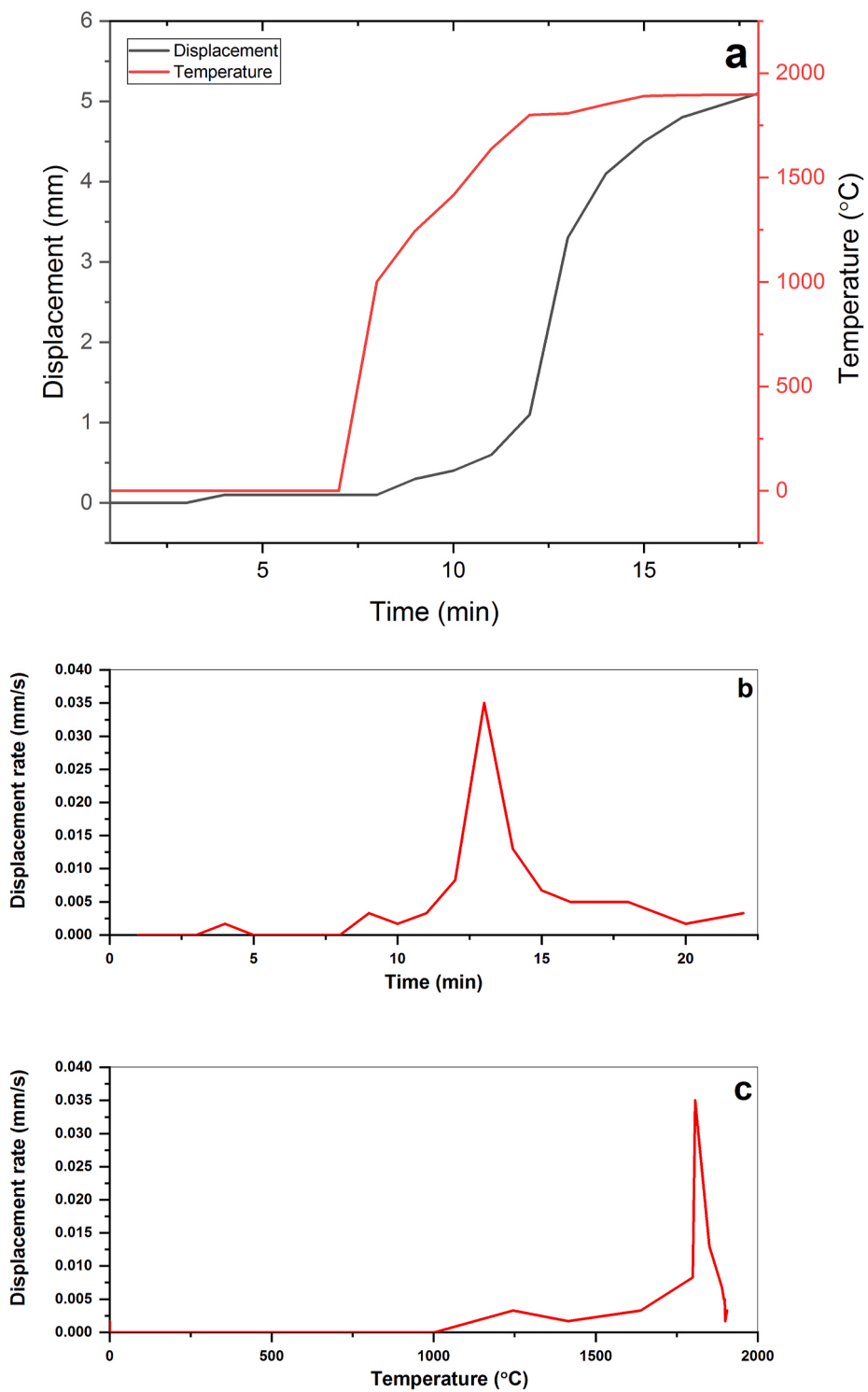


Fig. 14. (a) Displacement-time-temperature, (b) displacement rate-time, and (c) displacement rate-temperature curves of the sample sintered at 1900 °C.

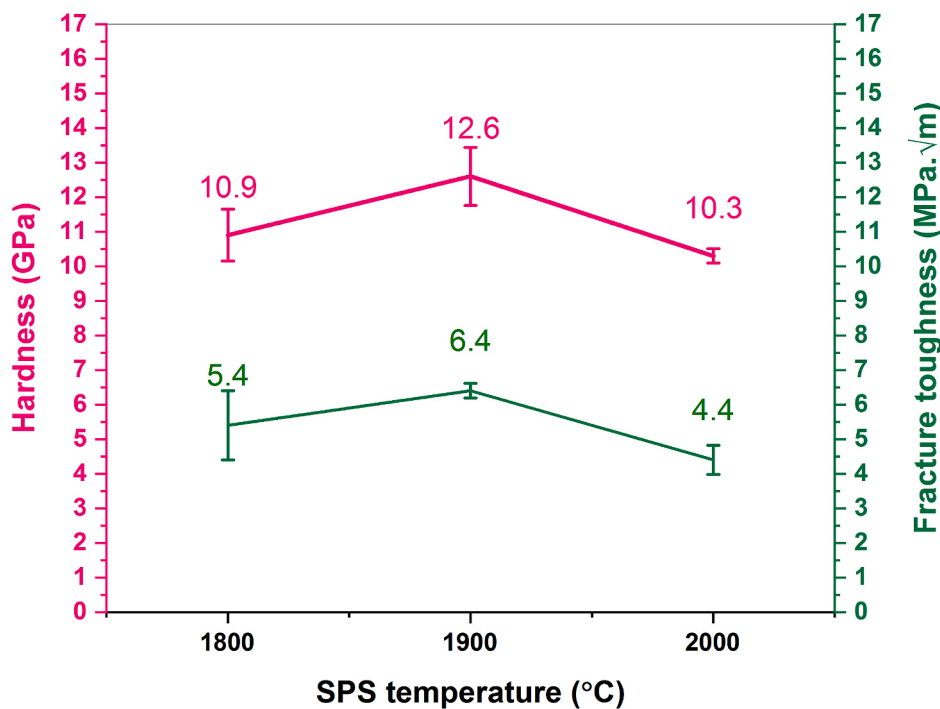


Fig. 15. The hardness and fracture toughness of the ZrB₂-5 wt% HEA samples sintered at various temperatures.

Table 2
Fracture toughness of ZrB₂ ceramics with various additives and sintering conditions.

Ceramic	Additive	Sintering method	Sintering temperature (°C)	Fracture toughness (MPa·m ^{1/2})	Ref.
ZrB ₂	Ni	HP	1850	3.4	[85]
ZrB ₂ -ZrC	La	SPS	1800	2.6	[38]
ZrB ₂	TiN	HP	1800	3.8	[5]
ZrB ₂	B ₄ C + Ni	HP	1850	4.5	[85]
ZrB ₂	SiC	RHP	1900	4	[86]
ZrB ₂	Graphene	SPS	1900	2.8	[87]
ZrB ₂	ZrH ₂	SPS	1900	4.3–5	[88]
ZrB ₂	Zr ₂ Al ₄ C ₅	SPS	1800	2.5–4.2	[89]

toughness values of the specimens sintered at various temperatures, are remarkably greater than those of the monolithic ZrB₂ ceramics [83,84]. Note that the FCC structure of the HEA caused higher plasticity and enhanced toughness of ceramics through the ductile phase mechanism [53].

Table 2 outlines a list of fracture toughness values reported for different additives in the ZrB₂ ceramics. A fracture toughness of 3.4 MPa m^{1/2} was reported for ZrB₂ ceramics, sintered by HP at 1850 °C, with the addition of 4 wt% Ni [85]. Although the sintering conditions are almost the same and the Ni additive is one of the main elements in the Ni₂₅Co₂₀Cu₁₀Fe₂₅Mn₂₀ HEA, the obtained fracture toughness with Ni addition is smaller than the fracture toughness values in the current research. Addition of 13 wt% B₄C and 4 wt% Ni to ZrB₂ ceramic, fabricated by HP at 1850 °C, resulted in a fracture toughness of 4.5 MPa m^{1/2} [85]. This value is almost equal to the lowest fracture toughness (4.4 MPa m^{1/2}) in the present research. Introducing La to ZrB₂-ZrC ceramic, processed by SPS at 1800 °C, led to a fracture toughness of ~2.6 MPa m^{1/2} [38], which is far lower than the results achieved for the ZrB₂-5 wt% HEA samples. A fracture toughness of 4 MPa m^{1/2} was reported for SiC added ZrB₂ ceramics manufactured by reactive HP at 1900 °C [86]. Such a value is 30% less than the one obtained for ZrB₂-5 wt% HEA SPSed at 1900 °C. Adding 5 wt% of TiN to ZrB₂ ceramic using HP process at

1800 °C resulted in 3.8 MPa m^{1/2} fracture toughness [5], which is lower than this parameter value for sample sintered at same sintering temperature at present work. Usage of graphene nanoplatelets as sintering aid for ZrB₂ ceramic, prepared by SPS at 1900 °C, resulted in 2.77 MPa m^{1/2} fracture toughness [87]. This value is far lower than the fracture toughness obtained at 1900 °C in the present work. Upon adding ZrH₂ to ZrB₂ ceramic, fabricated by SPS at 1900 °C, fracture toughness values of 4.3–5 MPa m^{1/2} were measured [88]. This result is lower than the fracture toughness value for the ZrB₂-HEA sample sintered at the same temperature. Fracture toughness values of 2.5–4.2 MPa m^{1/2} were reported for the ZrB₂ ceramic, fabricated via SPS at 1800 °C, upon adding Zr₂Al₄C₅ sintering aid [89]. This outcome is also far lower than the fracture toughness of 5.4 MPa m^{1/2} for the ZrB₂-HEA specimen SPSed at 1800 °C.

The secondary phases can prevent the crack growth and the movement of lattice dislocation by filling the pores. Also, due to the difference in the thermal expansion coefficients of the ceramic matrix (ZrB₂) and the secondary phase (HEA), when the sample is cooled, microcracks are formed at the interface of these two phases; these microcracks can cause the deviation of the crack path and increase the fracture toughness of the sample [53].

The crack growth paths were monitored to investigate the various toughening mechanisms (see Fig. 16). Several mechanisms including crack deflection, crack branching, crack bridging, secondary phase fracture, and crack trapping intensified the fracture toughness of the HEA-containing specimens compared to the monolithic ZrB₂ ceramics.

4. Conclusions

Nanostructure non-equimolar Ni₂₅Co₂₀Cu₁₀Fe₂₅Mn₂₀ high entropy alloy was used for the first time as a sintering aid for fabrication of ZrB₂ ultrahigh temperature ceramic using SPS process. The results of this research can be summarized as follows:

- ZrB₂-5 wt% HEA sample sintered at 1900 °C has a set of suitable properties such as relative density of 96%, hardness of 12.6 GPa and fracture toughness of 6.4 MPa m^{1/2}.

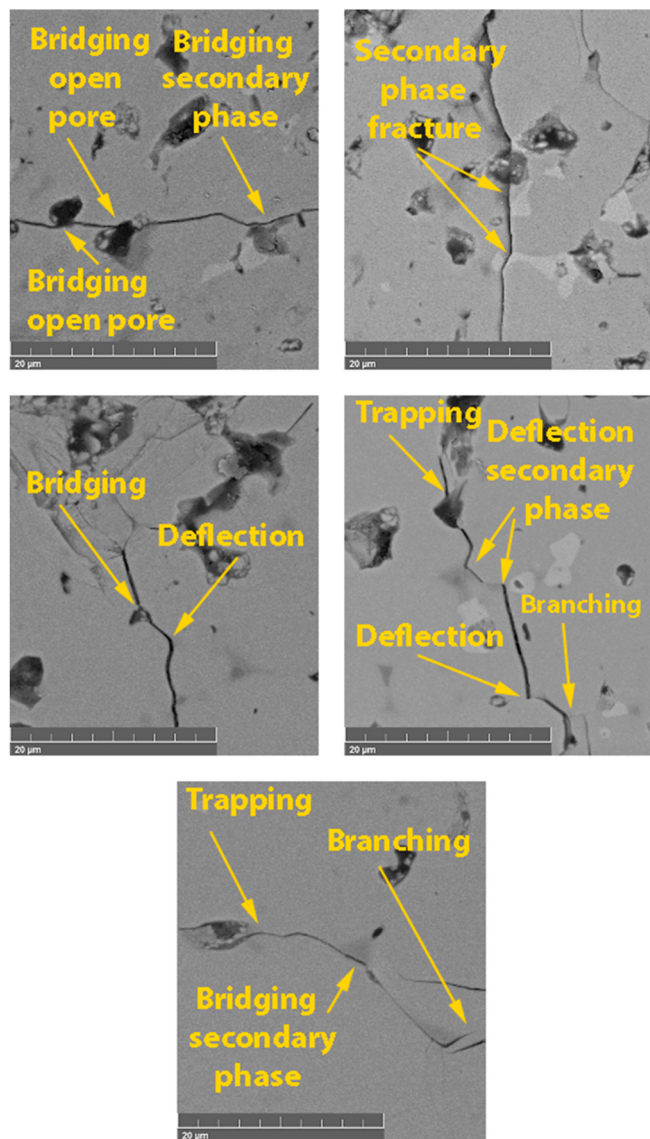


Fig. 16. FE-SEM images of the crack growth paths showing the toughening mechanisms in the sintered samples.

- In the XRD patterns, peaks of new secondary phases were identified in addition to ZrB₂ matrix including ZrC and ZrO₂. Based on the EDS maps and the history of the NiCoCuFeMn alloy, the Cu element separated from the HEA. The formation of CuB phase seemed possible.
- By calculating the crystallite size related to the ZrB₂ phase in the as-received, as-mixed, and as-sintered specimens, it was determined that even at the sintering temperature of 2000 °C, this parameter was lower than 100 nm, so the presence of the HEA in the system prevented significant grain growth.
- The presence of high entropy alloy with FCC structure boosted the fracture toughness based on the ductile phase toughening mechanism.

Declaration of competing interest

The authors declare that they have no known competing financial interests or personal relationships that could have appeared to influence the work reported in this paper.

Acknowledgments

We would like to express our sincere gratitude to Assistant Prof. Dr. Zohre Ahmadi from the University of Kyrenia in Cyprus for her invaluable assistance and dedication during the experiments and interpretation of the results presented in this paper. Her expertise and support were instrumental in shaping the outcome of this research.

References

- A. Emdadi, J. Watts, W.G. Fahrenholtz, G.E. Hilmas, M.A. Zaeem, Predicting effective fracture toughness of ZrB₂-based ultra-high temperature ceramics by phase-field modeling, *Mater. Des.* 192 (2020) 108713.
- N. Sadeghi, H. Aghajani, M. Akbarpour, Microstructure and tribological properties of in-situ TiC-Cu nanocomposites synthesized using different carbon sources (graphite, carbon nanotube and graphene) in the Cu-Ti-C system, *Ceram. Int.* 44 (2018) 22059–22067.
- D. Bannykh, A. Utkin, N. Baklanova, The peculiarities in oxidation behavior of the ZrB₂-SiC ceramics with chromium additive, *Int. J. Refract. Metals Hard Mater.* 84 (2019) 105023.
- N. Sadeghi, M. Akbarpour, H. Aghajani, A novel two-step mechanical milling approach and in-situ reactive synthesis to fabricate TiC/Graphene layer/Cu nanocomposites and investigation of their mechanical properties, *Mater. Sci. Eng., A* 734 (2018) 164–170.
- A. Shima, M. Kazemi, Influence of TiN addition on densification behavior and mechanical properties of ZrB₂ ceramics, *Synthes. Sinter.* 3 (2023) 46–53.
- M. Vajdi, S.M. Bagheri, F.S. Moghanlou, A.S. Khorrami, Numerical investigation of solar collectors as a potential source for sintering of ZrB₂, *Synthes. Sinter.* 1 (2021) 76–84.
- B.R. Golla, S.K. Thimmappa, Comparative study on microstructure and oxidation behaviour of ZrB₂-20 vol% SiC ceramics reinforced with Si₃N₄/Ta additives, *J. Alloys Compd.* 797 (2019) 92–100.
- Z. Balak, Shrinkage, hardness and fracture toughness of ternary ZrB₂-SiC-HfB₂ composite with different amount of HfB₂, *Mater. Chem. Phys.* 235 (2019) 121706.
- D. Medved, J. Balko, R. Sedláček, A. Kovalčíková, I. Šepa, A. Naughton-Duszová, E. Bączek, M. Podsiadlo, J. Dusza, Wear resistance of ZrB₂ based ceramic composites, *Int. J. Refract. Metals Hard Mater.* 81 (2019) 214–224.
- X. Jin, P. Li, C. Hou, X. Wang, X. Fan, C. Lu, G. Xiao, X. Shu, Oxidation behaviors of ZrB₂ based ultra-high temperature ceramics under compressive stress, *Ceram. Int.* 45 (2019) 7278–7285.
- J. Sonber, A. Suri, Synthesis and consolidation of zirconium diboride, *Adv. Appl. Ceram.* 110 (2011) 321–334.
- J. Zou, G.-J. Zhang, Z.-Y. Fu, In-situ ZrB₂-hBN ceramics with high strength and low elasticity, *J. Mater. Sci. Technol.* 48 (2020) 186–193.
- V. Iacobellis, A. Radhi, K. Behdinan, Discrete element model for ZrB₂-SiC ceramic composite sintering, *Compos. Struct.* 229 (2019) 111373.
- R. Hassan, S. Omar, K. Balani, Solid solutioning in ZrB₂ with HfB₂: effect on densification and oxidation resistance, *Int. J. Refract. Metals Hard Mater.* 84 (2019) 105041.
- S.-Q. Guo, Densification of ZrB₂-based composites and their mechanical and physical properties: a review, *J. Eur. Ceram. Soc.* 29 (2009) 995–1011.
- J.R. Fenter, Refractory diborides as engineering materials(Refractory diborides in oxidizing environments, considering mechanical strength, thermal stability, oxidation resistance, heat conductivity, thermal expansion, specific heat and electrical resistance), *SAMPE Q.* 2 (1971) 1–15.
- R. Telle, L. Sigl, K. Takagi, Boride-based Hard Materials, *Handbook of Ceramic Hard Materials*, 2000, pp. 802–945.
- D. Kalish, E.V. Clougherty, K. Kreder, Strength, fracture mode, and thermal stress resistance of HfB₂ and ZrB₂, *J. Am. Ceram. Soc.* 52 (1969) 30–36.
- W.G. Fahrenholtz, G.E. Hilmas, I.G. Talmi, J.A. Zaykoski, Refractory diborides of zirconium and hafnium, *J. Am. Ceram. Soc.* 90 (2007) 1347–1364.
- S. Chakraborty, P.K. Das, D. Ghosh, SPARK PLASMA SINTERING AND STRUCTURAL PROPERTIES OF ZrB₂ BASED CERAMICS: a review, *Rev. Adv. Mater. Sci.* (2016) 44.
- A. Rezapour, Z. Balak, Fracture toughness and hardness investigation in ZrB₂-SiC-ZrC composite, *Mater. Chem. Phys.* 241 (2020) 122284.
- S.K. Thimmappa, B.R. Golla, V.B. Prasad, B. Majumdar, B. Basu, Phase stability, hardness and oxidation behaviour of spark plasma sintered ZrB₂-SiC-Si₃N₄ composites, *Ceram. Int.* 45 (2019) 9061–9073.
- F.S. Moghanlou, M. Vajdi, A. Motallebzadeh, J. Sha, M. Shokouhimehr, M.S. Asl, Numerical analyses of heat transfer and thermal stress in a ZrB₂ gas turbine stator blade, *Ceram. Int.* 45 (2019) 17742–17750.
- R. Eatemadi, Z. Balak, Investigating the effect of SPS parameters on densification and fracture toughness of ZrB₂-SiC nanocomposite, *Ceram. Int.* 45 (2019) 4763–4770.
- M.S. Kumar, S.R. Begum, M. Vasumathi, C.C. Nguyen, Q. Van Le, Influence of molybdenum content on the microstructure of spark plasma sintered titanium alloys, *Synthes. Sinter.* 1 (2021) 41–47.
- E. Dodi, Z. Balak, H. Kafashan, Oxidation-affected zone in the sintered ZrB₂-SiC-HfB₂ composites, *Synthes. Sinter.* 2 (2022) 31–36.
- H. Istgaldi, M. Mehrabian, F. Kazemi, B. Nayebi, Reactive spark plasma sintering of ZrB₂-TiC composites: role of nano-sized carbon black additive, *Synthes. Sinter.* 2 (2022) 67–77.

- [28] M. Sakkaki, M. Naderi, M. Vajdi, F.S. Moghanlou, A.T. Beris, A simulative approach to obtain higher temperatures during spark plasma sintering of ZrB₂ ceramics by geometry optimization, *Synthes. Sinter.* 3 (2023) 248–258.
- [29] M.S. Asl, M.G. Kakroud, F. Golestan-Fard, H. Nasiri, A Taguchi approach to the influence of hot pressing parameters and SiC content on the sinterability of ZrB₂-based composites, *Int. J. Refract. Metals Hard Mater.* 51 (2015) 81–90.
- [30] B. Nayebi, M.S. Asl, M.G. Kakroud, M. Shokouhimehr, Temperature dependence of microstructure evolution during hot pressing of ZrB₂-30 vol.% SiC composites, *Int. J. Refract. Metals Hard Mater.* 54 (2016) 7–13.
- [31] X. Sun, W. Han, Q. Liu, P. Hu, C. Hong, ZrB₂-ceramic toughened by refractory metal Nb prepared by hot-pressing, *Mater. Des.* 31 (2010) 4427–4431.
- [32] M.J. Mousavi, M. Zakeri, M. Rahimipour, E. Amini, Mechanical properties of pressure-less sintered ZrB₂ with molybdenum, iron and carbon additives, *Mater. Sci. Eng., A* 613 (2014) 3–7.
- [33] S.K. Mishra, S.K. Das, A.K. Ray, P. Ramachandrarao, Effect of Fe and Cr addition on the sintering behavior of ZrB₂ produced by self-propagating high-temperature synthesis, *J. Am. Ceram. Soc.* 85 (2002) 2846–2848.
- [34] H. Wang, D. Chen, C.-A. Wang, R. Zhang, D. Fang, Preparation and characterization of high-toughness ZrB₂/Mo composites by hot-pressing process, *Int. J. Refract. Metals Hard Mater.* 27 (2009) 1024–1026.
- [35] J. Meléndez-Martínez, A. Domínguez-Rodríguez, F. Monteverde, C. Melandri, G. De Portu, Characterisation and high temperature mechanical properties of zirconium boride-based materials, *J. Eur. Ceram. Soc.* 22 (2002) 2543–2549.
- [36] A. Khanra, M. Godkhini, Effect of Ni additives on pressureless sintering of SHS ZrB₂, *Adv. Appl. Ceram.* 104 (2005) 273–276.
- [37] T. Venkateswaran, B. Basu, G. Raju, D.-Y. Kim, Densification and properties of transition metal borides-based cermets via spark plasma sintering, *J. Eur. Ceram. Soc.* 26 (2006) 2431–2440.
- [38] K.H. Kim, K.B. Shim, The effect of lanthanum on the fabrication of ZrB₂–ZrC composites by spark plasma sintering, *Mater. Char.* 50 (2003) 31–37.
- [39] A. Purwar, R. Mukherjee, K. Ravikumar, S. Ariharan, N.K. Gopinath, B. Basu, Development of ZrB₂–SiC–Ti by multi stage spark plasma sintering at 1600° C, *J. Ceram. Soc. Jpn.* 124 (2016) 393–402.
- [40] E. Ghasali, M.S. Asl, Microstructural development during spark plasma sintering of ZrB₂–SiC–Ti composite, *Ceram. Int.* 44 (2018) 18078–18083.
- [41] R. Li, M. Wang, T. Yuan, B. Song, Y. Shi, Microstructural modification of laser-deposited high-entropy CrFeCoNiMoWC alloy by friction stir processing: nanograin formation and deformation mechanism, *Metall. Mater. Trans. A* 48 (2017) 841–854.
- [42] D.B. Miracle, O.N. Senkov, A critical review of high entropy alloys and related concepts, *Acta Mater.* 122 (2017) 448–511.
- [43] S. Gorsse, D.B. Miracle, O.N. Senkov, Mapping the world of complex concentrated alloys, *Acta Mater.* 135 (2017) 177–187.
- [44] S. Mamnooni, E. Borhani, H. Heydari, Is synthesizing a Cu35Co35Ni20Ti5Al5 high-entropy alloy beyond the rules of solid-solution formation? *Synthes. Sinter.* 3 (2023) 226–233.
- [45] F. Otto, Y. Yang, H. Bei, E.P. George, Relative effects of enthalpy and entropy on the phase stability of equiatomic high-entropy alloys, *Acta Mater.* 61 (2013) 2628–2638.
- [46] J.W. Yeh, S.K. Chen, S.J. Lin, J.Y. Gan, T.S. Chin, T.T. Shun, C.H. Tsau, S.Y. Chang, Nanostructured high-entropy alloys with multiple principal elements: novel alloy design concepts and outcomes, *Adv. Eng. Mater.* 6 (2004) 299–303.
- [47] Y. Deng, C.C. Tasan, K.G. Pradeep, H. Springer, A. Kostka, D. Raabe, Design of a twinning-induced plasticity high entropy alloy, *Acta Mater.* 94 (2015) 124–133.
- [48] K.-Y. Tsai, M.-H. Tsai, J.-W. Yeh, Sluggish diffusion in co-cr-fe-mn-ni high-entropy alloys, *Acta Mater.* 61 (2013) 4887–4897.
- [49] F. Otto, A. Dlouhý, C. Somsen, H. Bei, G. Eggeler, E.P. George, The influences of temperature and microstructure on the tensile properties of a CoCrFeMnNi high-entropy alloy, *Acta Mater.* 61 (2013) 5743–5755.
- [50] C.-S. Chen, C.-C. Yang, H.-Y. Chai, J.-W. Yeh, J.L.H. Chau, Novel cermet material of WC/multi-element alloy, *Int. J. Refract. Metals Hard Mater.* 43 (2014) 200–204.
- [51] M. Ruiz-Esparza-Rodríguez, C. Garay-Reyes, I. Estrada-Guel, R. Martínez-Sánchez, Microstructural, structural and mechanical behavior of WC-based hardmetals bonded with high and medium entropy alloys, *Microsc. Microanal.* 25 (2019) 1794–1795.
- [52] G. Zhu, Y. Liu, J. Ye, Early high-temperature oxidation behavior of Ti (C, N)-based cermets with multi-component AlCoCrFeNi high-entropy alloy binder, *Int. J. Refract. Metals Hard Mater.* 44 (2014) 35–41.
- [53] M. Zhang, R. Li, T. Yuan, X. Feng, L. Li, S. Xie, Q. Weng, Densification and properties of B4C-based ceramics with CrMnFeCoNi high entropy alloy as a sintering aid by spark plasma sintering, *Powder Technol.* 343 (2019) 58–67.
- [54] E. Rogal, D. Kalita, A. Tarasek, P. Bobrowski, F. Czerwinski, Effect of SiC nanoparticles on microstructure and mechanical properties of the CoCrFeMnNi high entropy alloy, *J. Alloys Compd.* 708 (2017) 344–352.
- [55] W. Ji, J. Zhang, W. Wang, F. Zhang, Y. Wang, Z. Fu, Fabrication and properties of TiB₂-based cermets by spark plasma sintering with CoCrFeNiTiAl high-entropy alloy as sintering aid, *J. Eur. Ceram. Soc.* 35 (2015) 879–886.
- [56] G. Zhu, Y. Liu, J. Ye, Fabrication and properties of Ti (C, N)-based cermets with multi-component AlCoCrFeNi high-entropy alloys binder, *Mater. Lett.* 113 (2013) 80–82.
- [57] C.-M. Lin, C.-W. Tsai, S.-M. Huang, C.-C. Yang, J.-W. Yeh, New TiC/CoCrFeNiTi cermet with slow TiC coarsening during sintering, *JOM: J. Miner. Met. Mater. Soc.* (2014) 66.
- [58] S. Zhang, Y. Sun, B. Ke, Y. Li, W. Ji, W. Wang, Z. Fu, Preparation and characterization of TiB₂-(supra-nano-dual-phase) high-entropy alloy cermet by spark plasma sintering, *Metals* 8 (2018) 58.
- [59] P.-F. Zhou, D.-H. Xiao, T.-C. Yuan, Comparison between ultrafine-grained WC–Co and WC–HEA-cemented carbides, *Powder Metall.* 60 (2017) 1–6.
- [60] G. Anstis, P. Chantikul, B.R. Lawn, D. Marshall, A critical evaluation of indentation techniques for measuring fracture toughness: I, direct crack measurements, *J. Am. Ceram. Soc.* 64 (1981) 533–538.
- [61] L.F. Nielsen, Elasticity and damping of porous materials and impregnated materials, *J. Am. Ceram. Soc.* 67 (1984) 93–98.
- [62] I. FarahBakhsh, R. Antiochia, H.W. Jang, Pressureless sinterability study of ZrB₂–SiC composites containing hexagonal BN and phenolic resin additives, *Synthes. Sinter.* 1 (2021) 99–104.
- [63] A. Sharma, D.B. Karunakar, Influence of MgO addition on mechanical and ablation characteristics of ZrB₂–SiC composites developed through microwave sintering, *J. Mater. Sci.* 56 (2021) 17979–17993.
- [64] S.H. Shafagh, S. Jafargholinejad, S. Javadian, Beneficial effect of low BN additive on densification and mechanical properties of hot-pressed ZrB₂–SiC composites, *Synthes. Sinter.* 1 (2021) 69–75.
- [65] L. He, Y. Sun, Q. Meng, B. Liu, J. Wu, X. Zhang, Enhanced oxidation properties of ZrB₂–SiC composite with short carbon fibers at 1600 C, *Ceram. Int.* 47 (2021) 15483–15490.
- [66] N.S. Peighambardoust, C. Çevik, T. Assar, S. Jung, S.Y. Lee, J.H. Cha, Pulsed electric current sintering of TiB₂-based ceramics using nitride additives, *Synthes. Sinter.* 1 (2021) 28–33.
- [67] W. Ji, Z. Fu, W. Wang, H. Wang, J. Zhang, Y. Wang, F. Zhang, Mechanical alloying synthesis and spark plasma sintering consolidation of CoCrFeNiAl high-entropy alloy, *J. Alloys Compd.* 589 (2014) 61–66.
- [68] C. Wang, W. Ji, Z. Fu, Mechanical alloying and spark plasma sintering of CoCrFeNiMnAl high-entropy alloy, *Adv. Powder Technol.* 25 (2014) 1334–1338.
- [69] P. Villars, K. Cenzual, *Space Groups (166) R-3m-(160) R3m*, Springer, 2008.
- [70] R. Sonkusare, K. Biswas, W. Gan, H. Brokmeier, N. Gurao, Texture evolution during hot compression of CoCuFeMnNi complex concentrated alloy using neutron diffraction and crystal plasticity simulations, *Trans. Indian Inst. Met.* 75 (2022) 3061–3066.
- [71] J. Fiocchi, R. Casati, A. Tuissi, C.A. Biffi, Laser beam welding of CoCuFeMnNi high entropy alloy: processing, microstructure, and mechanical properties, *Adv. Eng. Mater.* 24 (2022) 2200523.
- [72] R. Sonkusare, P.D. Janani, N. Gurao, S. Sarkar, S. Sen, K. Pradeep, K. Biswas, Phase equilibria in equiatomic CoCuFeMnNi high entropy alloy, *Mater. Chem. Phys.* 210 (2018) 269–278.
- [73] S. Mamnooni, E. Borhani, D. Bovand, In-situ synthesis of aluminum matrix composite from Al–NiO system by mechanical alloying, *Met. Mater. Int.* 27 (2021) 1631–1638.
- [74] R.M.d. Rocha, F.F. Sene, M.d.O. Juliani, C.O. Davi, Effect of ZrB₂ particle size on pressureless sintering of ZrB₂–B-SiC composites, *J. Aero. Technol. Manag.* (2019) 11.
- [75] M.J. Zamharir, M. Zakeri, M. Razavi, M.S. Asl, Effect of co-addition of WC and MoSi₂ on the microstructure of ZrB₂–SiC–Si composites, *Int. J. Refract. Metals Hard Mater.* 103 (2022) 105775.
- [76] A. Babapoor, M.S. Asl, Z. Ahmadi, A.S. Namini, Effects of spark plasma sintering temperature on densification, hardness and thermal conductivity of titanium carbide, *Ceram. Int.* 44 (2018) 14541–14546.
- [77] J. Chen, R. Pippin, T. Hebesberger, O. Kolednik, The fracture behaviour of intermetallic TiAl alloys with and without warm pre-stressing, *Int. J. Fract.* 113 (2002) 327–343.
- [78] S.C. Zhang, G.E. Hilmas, W.G. Fahrenholtz, Pressureless sintering of ZrB₂–SiC ceramics, *J. Am. Ceram. Soc.* 91 (2008) 26–32.
- [79] M. Ikegami, S. Guo, Y. Kagawa, Densification behavior and microstructure of spark plasma sintered ZrB₂-based composites with SiC particles, *Ceram. Int.* 38 (2012) 769–774.
- [80] Z. Balak, M. Zakeri, M. Rahimipour, E. Salahi, H. Nasiri, Effect of open porosity on flexural strength and hardness of ZrB₂-based composites, *Ceram. Int.* 41 (2015) 8312–8319.
- [81] A.L. Chamberlain, W.G. Fahrenholtz, G.E. Hilmas, Pressureless sintering of zirconium diboride, *J. Am. Ceram. Soc.* 89 (2006) 450–456.
- [82] Z. Balak, M.S. Asl, M. Azizieh, H. Kafashan, R. Hayati, Effect of different additives and open porosity on fracture toughness of ZrB₂–SiC-based composites prepared by SPS, *Ceram. Int.* 43 (2017) 2209–2220.
- [83] L. Xu, Y. Yang, S. Wang, M. Li, J. Xu, Y. Qian, J. Zuo, D. Zhang, Improved both mechanical and anti-oxidation performances of ZrB₂–SiC ceramics with molybdenum disilicide addition, *Mater. Chem. Phys.* 223 (2019) 53–59.
- [84] J. Sonber, T.C. Murthy, C. Subramanian, S. Kumar, R. Fotedar, A. Suri, Investigations on synthesis of ZrB₂ and development of new composites with HfB₂ and TiSi₂, *Int. J. Refract. Metals Hard Mater.* 29 (2011) 21–30.
- [85] F. Monteverde, A. Bellosi, S. Giuccardi, Processing and properties of zirconium diboride-based composites, *J. Eur. Ceram. Soc.* 22 (2002) 279–288.
- [86] G.J. Zhang, Z.Y. Deng, N. Kondo, J.F. Yang, T. Ohji, Reactive hot pressing of ZrB₂–SiC composites, *J. Am. Ceram. Soc.* 83 (2000) 2330–2332.
- [87] G.B. Yadukulakrishnan, S. Karumuri, A. Rahman, R.P. Singh, A.K. Kalkan, S. P. Harimkar, Spark plasma sintering of graphene reinforced zirconium diboride ultra-high temperature ceramic composites, *Ceram. Int.* 39 (2013) 6637–6646.
- [88] S. Ran, S.G. Huang, O. Van der Biest, J. Vleugels, High-strength ZrB₂-based ceramics prepared by reactive pulsed electric current sintering of ZrB₂–ZrH₂ powders, *J. Eur. Ceram. Soc.* 32 (2012) 2537–2543.
- [89] Q. Guo, J. Li, Q. Shen, L. Zhang, Preparation, microstructure, and mechanical properties of ZrB₂-based ceramics with layered Zr2Al4C5 inclusions, *Ceram. Int.* 39 (2013) 2215–2222.